ACS NANO
Cite This: ACS Nano XXXX, XXX, XXX−XXX
www.acsnano.org

ARTICLE

Self-Powered Multifunctional Motion Sensor Enabled by Magnetic-Regulated Triboelectric Nanogenerator

Zhiyi Wu,[†,‡,⊥] Wenbo Ding,[†,⊥] Yejing Dai,[†,⊥] Kai Dong,[†] Changsheng Wu,[†] Lei Zhang,[†] Zhiming Lin,[†] Jia Cheng,[†] and Zhong Lin Wang*[,†,§]

[†]School of Materials Science and Engineering, Georgia Institute of Technology, Atlanta, Georgia 30332-0245, United States
[‡]Engineering Research Center for Mechanical Testing Technology and Equipment of Ministry of Education, Chongqing University of Technology, Chongqing 400054, China
[§]Beijing Institute of Nanoenergy and Nanosystems, Chinese Academy of Sciences, Beijing 100083, China

Supporting Information

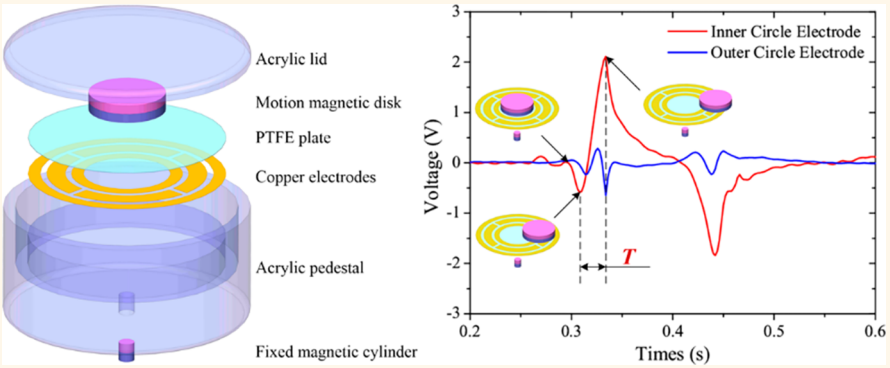

ABSTRACT: **With the fast development of the Internet of Things, the requirements of system miniaturization and integration have accelerated research on multifunctional sensors. Based on the triboelectric nanogenerator, a self-powered multifunctional motion sensor (MFMS) is proposed in this work, which is capable of detecting the motion parameters, including direction, speed, and acceleration of linear and rotary motions, simultaneously. The MFMS consists of a triboelectric nanogenerator (TENG) module, a magnetic regulation module, and an acrylic shell. The TENG module is formed by placing a free-standing magnetic disk (MD) on a polytetrafluorethylene (PTFE) plate with six copper electrodes. The movement of the MFMS causes the MD to slide on the PTFE plate and hence excites the electrodes to produce a voltage output. The carefully designed six copper electrodes (an inner circle electrode, an outer circle electrode, and four arc electrodes between them) can distinguish eight directions of movement with the acceleration and determine the rotational speed and direction as well. Besides, the magnetic regulation module is applied here by fixing a magnetic cylinder (MC) in the shell, right under the center of the PTFE plate. Due to the magnetic attraction applied by the MC, the MD will automatically return to the center to prepare for the next round of detection, which makes the proposed sensor much more applicable in practice.**

KEYWORDS: *motion sensor, triboelectric nanogenerator, self-powered sensor, magnetic regulation, multifunction*

Motion sensors, which can measure the displacement, speed, acceleration, direction, and other motion-related parameters, have played an important and irreplaceable role in aerospace, driverless vehicles, large mechanical structure testing, smart phones, and many other fields. The existing commercial motion sensors include encoders,[1−3] synchros and resolvers,[4−6] accelerometers,[7−9] gyroscopes,[10,11] and compasses.[12,13] Despite the superior performance, the commercial ones usually have a single function, which only work at specific conditions and sometimes may not fulfill the requirements of system miniaturization and integration. In this context, multifunctional sensors have attracted more and more interest from both academia and industry.[14−20] However, the current multifunctional sensors are usually the combination of several single-functional sensors that actually work independently.

Received: February 28, 2018
Accepted: May 25, 2018
Published: May 25, 2018

DOI: 10.1021/acsnano.8b01589
ACS Nano XXXX, XXX, XXX−XXX

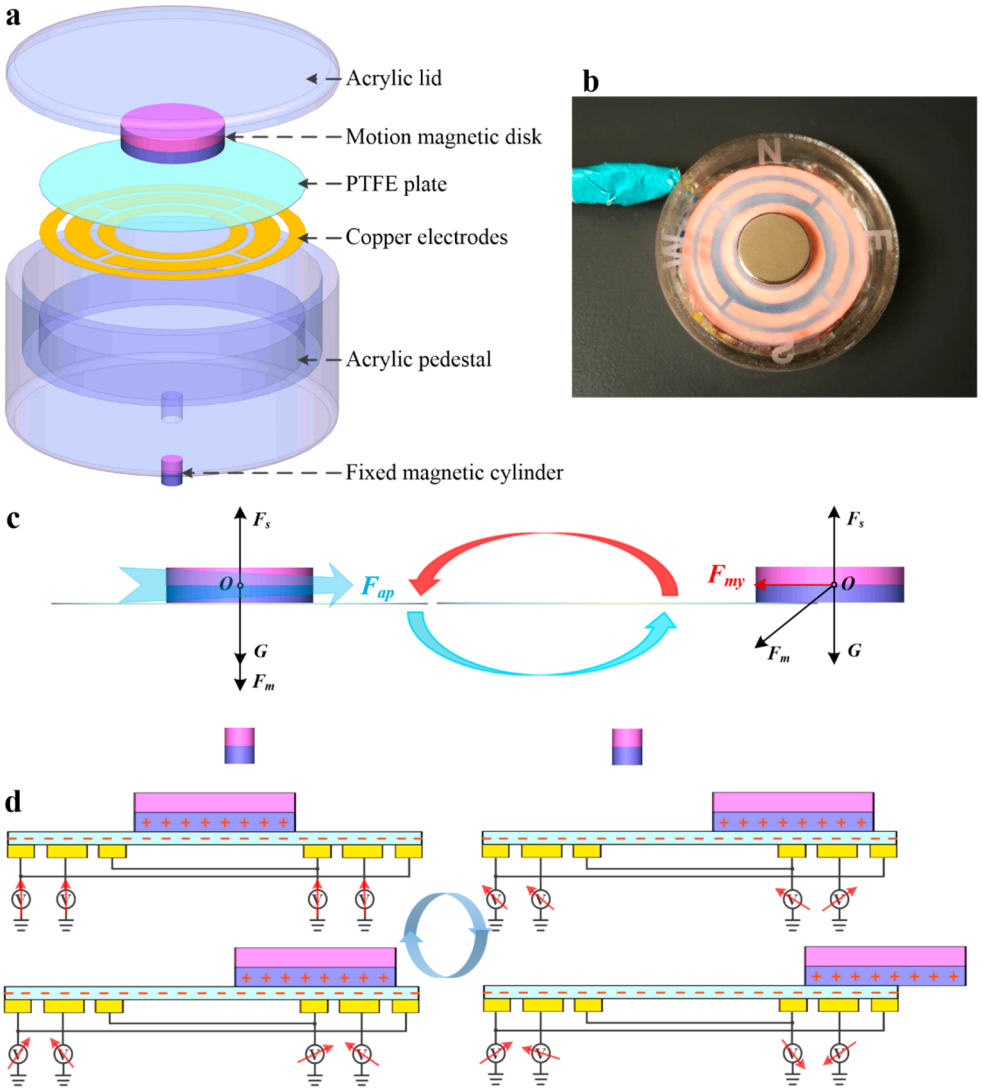

Figure 1. Structure and illustration of the working principle of a self-powered multifunctional motion sensor. (a) Schematic diagram of the MFMS. (b) Photograph of the MFMS. (c) Mechanics analysis diagram of the magnetic regulation system with the MD above the MC. (d) Schematic illustration of the working principle of the MFMS to produce electricity.

On the other hand, with the development of the Internet of Things, the sensors are expected to continuously work for a long time and without maintenance.[21] So, the existing commercial motion sensors that require external power to sensing will not be able to meet the requirements. There are some researchers using the piezoelectric effect to build accelerometers, which is a milestone for self-powered sensing.[8,9] Nevertheless, the output signal of the piezoelectric sensor is relatively small and might be influenced by the environmental noise. Triboelectric nanogenerators (TENGs), invented by Wang *et al.* in 2012, have proven to be a possible solution for both energy harvesting and self-powered sensing.[22−26] Specifically, the TENGs have been successfully applied to construct self-powered motion sensors.[27−33] For example, a spherical TENG with a single electrode was designed to work as a self-powered acceleration sensor, which can detect the existence of any excitation but cannot distinguish its direction.[27] Based on three independent TENGs, a self-powered 3D acceleration sensor can be used to measure vector acceleration in any direction.[33] Unfortunately, the volume of the sensor has been inevitably significantly increased. To our best knowledge, there is no research on a real multifunctional motion sensor based on a TENG. Moreover, a magnet has been successfully used to enhance the output performance of TENGs,[34−36] which could give some guidance to the design of a real multifunctional motion sensor.

In this work, a self-powered multifunctional motion sensor (MFMS) with magnet regulation based on a TENG is presented, which is capable of detecting the motion parameters, including direction, speed, and acceleration, of linear and rotary motions. The MFMS consists of a TENG module, a magnetic regulation module, and an acrylic shell. The TENG module is formed by placing a free-standing magnetic disk (MD) on a polytetrafluorethylene (PTFE) plate with six copper electrodes (an inner circle electrode, an outer circle electrode, and four arc electrodes between them). The movement of the MFMS will cause the MD to slide on the PTFE plate and hence excites the electrodes to produce a voltage output. Voltage waveforms acquired from the four arc electrodes are used to measure the directions of both linear and rotational motions, as well as the rotational speed. From the voltage waveforms of the inner and outer circle electrodes, a time feature can be extracted to

DOI: 10.1021/acsnano.8b01589
ACS Nano XXXX, XXX, XXX−XXX

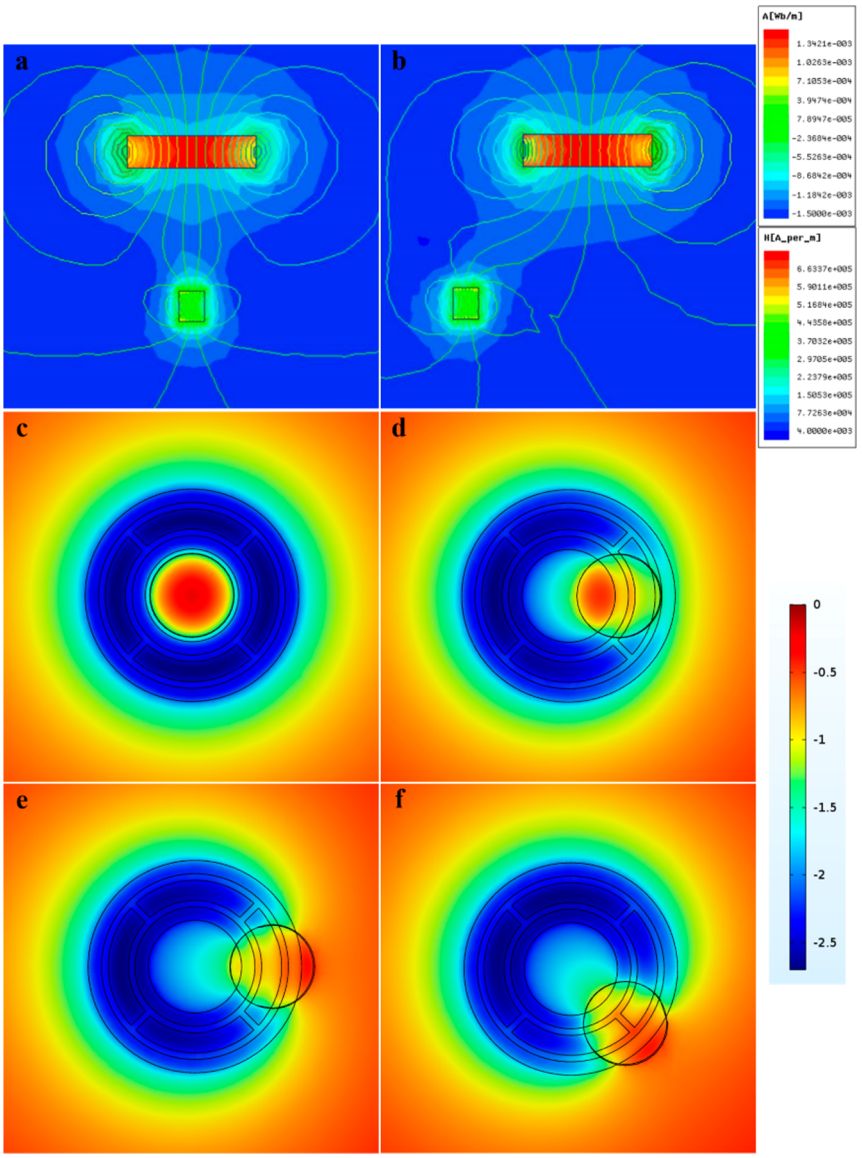

Figure 2. Simulation results of the magnetic regulation system and six electrodes of the MFMS using Maxwell 14.0 and COMSOL Multiphysics 5.3, respectively. (a, b) Magnetic distributions of the MD at the original and balanced place and the unbalanced place, respectively. (c) Electrostatic potential distribution of the MD at the center place. (d–f) Electrostatic potential distributions of the MD above the inner circle electrode, an arc electrode, and the middle place between two arc electrodes, respectively.

determine the acceleration of the linear motion along any two-dimensional direction. The MD together with a fixed magnetic cylinder (MC) implanted in the shell forms the magnetic regulation system. With the magnetic attraction from the MC, the MD can always come back to the center after each movement, which will guarantee the detection accuracy of the next movement. Theoretical analysis and experimental tests have been done to demonstrate the feasibility and effectiveness of the MFMS.

RESULTS AND DISCUSSION

The structure diagram of the self-powered multifunctional motion sensor and its entity are demonstrated in Figure 1a,b and Figure S1. The diameter and height of the MFMS are 40 mm and 19 mm, respectively. The volume of the MFMS is about 23.88 cm^3. The shell is made of acrylic, which is accurately cut by a laser cutter. In the MFMS, the TENG is composed of an MD and a friction layer constituted by a PTFE plate adhered by six copper electrodes. The dimensions of the friction layer are shown in Figure S2a. The electrodes include an inner circle electrode, an outer circle electrode, and arc electrodes between them. It should be noted here that the resolution of the MFMS can be improved by increasing the number of arc electrodes. Considering the trade-off among the robustness, miniaturization, and the complexity of the data processing part, the number of arc electrodes is specified as four. The four arc electrodes are denoted as North-E, East-E, South-E, and West-E, respectively. The diameter of the PTFE plate equals the external diameter of the outer circle electrode, which is 32 mm. Besides, the MD is also part of a magnetic regulation system, the sizes of which are described in Figure S2b. The diameters of the MD and MC are 12.5 mm and 2.54 mm, respectively. The height of both magnets (NdFeB, N38) is 3 mm. The magnetic attraction between the MD and MC (F_m) has a direct influence on the output performance of the MFMS. Under the determined dimensions and material of the MD and

DOI: 10.1021/acsnano.8b01589
ACS Nano XXXX, XXX, XXX–XXX

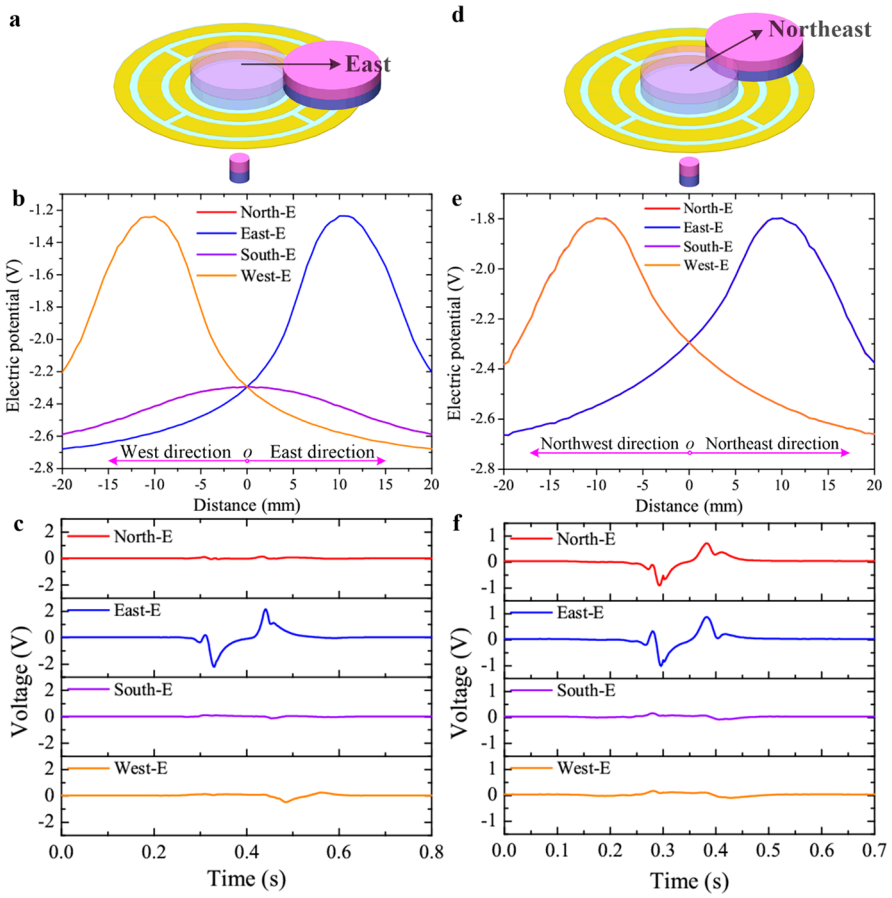

Figure 3. Working principle of linear motion direction measurement. (a) Schematic diagrams of the MD moving along the east direction. (b) Simulation results of four arc electrodes' electrostatic potential with the MD moving from west to east. (c) Voltage waveforms of four arc electrodes with the MD moving along the east direction. (d) Schematic diagrams of the MD moving along the northeast direction. (e) Simulation results of four arc electrodes' electrostatic potential with the MD moving from northwest to northeast. (f) Voltage waveforms of four arc electrodes with the MD moving along the northeast direction.

MC, the F_m can be optimized by adjusting the distance between the two magnets (d_m), as shown in Figure S3a. The vertical component of the magnetic pull of the MC (F_{mz}) is inversely proportional to d_m. A larger F_{mz} will increase the demand of the excitation. At the same time, a smaller F_{mz} will increase the height of the MFMS. Hence, d_m is specified as 10.5 mm under the consideration of the trade-off. The mechanics analysis diagram of the magnetic regulation system is illustrated in Figure 1c. When there is no excitation, the MD will always stay in the center of the PTFE plate due to the F_m. Under this condition, the gravity (G), F_m, and the supporting force (F_s) are all along the vertical direction ($G + F_m = F_s$). The excitations from any orientation except along the vertical direction will apply a horizontal force (F_{ap}) to break the balance, which forces the MD to slide on the PTFE plate. As F_m always points to the MC, with the movement of the MD, the horizontal component of F_m (F_{my}) will drive the MD back to the center. In those processes, according to the triboelectric effect, the open-circuit voltages can be detected on those electrodes, which are schematically displayed in Figure 1d. When the MD slides on the PTFE plate, owing to the different triboelectric polarity of the PTFE and Ni coating around the magnet, the electrons will transfer from the Ni coating to the PTFE plate, rendering them with positive and negative charges in the saturated state, respectively. The charges on their surfaces cannot be conducted away or neutralized in the measurement process. Hence, the Ni coating can be regarded as an equipotential surface. Then based on electrostatic induction, the open-circuit voltages of six electrodes will be changed with the movement of the MD.

To obtain a more quantitative understanding of the magnetic regulation system, a finite-element model simulation is performed using Maxwell 14.0. In Figure 2a, the magnetic field and magnetic induction line distributions of the magnetic regulation system are center symmetric. No matter where the MD is, the magnetic field will always be mainly concentrated at the area between the MD and MC, which is demonstrated in Figure 2b. That is to say, once the MD is off-center, the magnetic attraction from the MC will apply a centripetal force (F_{my}) to pull it back. The relationship between F_{my} and the distance from the center of the MD (d) is plotted in Figure S3b. With the increasing of d, F_{my} could reach an extreme value. This requires that the diameter of the shell cannot be too large. A suitable diameter ensures F_{my} can always pull the MD back to the center. Consequently, when designing the shell, except the demands of the PTFE plate, F_{my} should be taken into account as well. Figure 2c–f describe the electrostatic voltage distributions with the MD moving to different places by simulating in COMSOL Multiphysics 5.3. Those demonstrated the pattern of electrostatic potential distribution when the moving MD is regarded as an equipotential body. Thus, through analysis of the open-circuit voltage of electrodes, the mode and parameters of the MD's motion can be detected.

DOI: 10.1021/acsnano.8b01589
ACS Nano XXXX, XXX, XXX–XXX

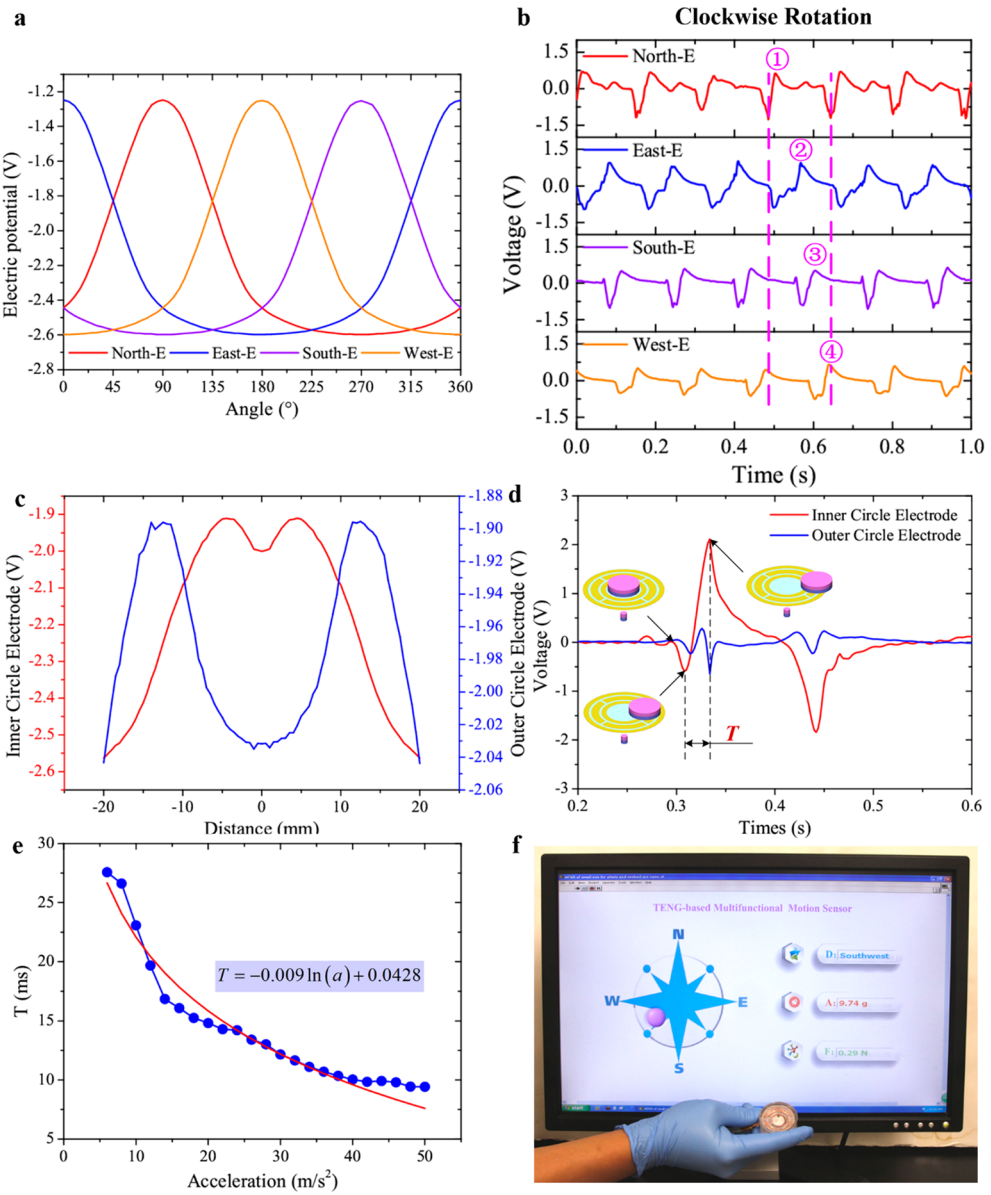

Figure 4. Working principle of rotational parameters and linear acceleration measurement and the applications of the MFMS. (a, b) Simulation results of electrostatic potential and voltage waveforms of four arc electrodes with MD rotation along the clockwise direction. (c, d) Simulation results of electrostatic potential and voltage waveforms of inner and outer circle electrodes with the MD with linear motion along any direction. (e) Relationship between the time and acceleration. (f) Application of the MFMS.

Under an external linear excitation, the MD will perform a linear motion accordingly. The schematic diagram of movement along the east direction is shown in Figure 3a. Figure 3b describes the simulation results of four arc electrodes' electrostatic potential with the MD moving from west to east. In this situation, the potential of the West-E and East-E will have the peak value successively, while the potential values of the North-E and South-E are relatively small and stay the same. That is to say, when the MD is moving toward any arc electrode, the potential of the target electrode should demonstrate a large and peak value, and the two adjacent electrodes have the same electrostatic potential of small magnitude. This has been demonstrated by the experimental results shown in Figure 3c. When the MD is moving along the east direction, the open-circuit voltage of the East-E is much larger than that of the other arc electrodes. So, four linear motion directions can be easily distinguished by finding the largest open-circuit voltage of the arc electrodes. Besides, the output performance of the MFMS with the MD moving along the central line between two adjacent arc electrodes, like moving along the northeast direction shown in Figure 3d, has been studied. The simulation results in Figure 3e indicate that the North-E and East-E have the same electrostatic potential; so do the South-E and West-E, while the two group electrodes have the opposite output performance. These have been further proved by the experimental results in Figure 3f. When the MD is moving along the northeast direction, the North-E and the East-E have almost the same open-circuit voltages, which are much larger than those of the South-E and West-E. In this way, eight linear motion directions can be easily measured with the proposed MFMS.

For clearly exhibiting the internal structure of the MFMS and observing the motion state of the MD, the shell is made of transparent acrylic and the MD is specified above the MC. But

DOI: 10.1021/acsnano.8b01589
ACS Nano XXXX, XXX, XXX−XXX

the mechanics analysis shown in Figure 1c is not a unique situation of the MFMS. Consequently, the MD also can be placed under the MC; that is, the end near the MD also can be used as the bottom of the MFMS. The mechanics analysis of this situation is shown in Figure S4. When there are no excitations, the MD also will always stay on the center of the PTFE plate due to F_m. Through adjusting F_m, the MD can be suspended near the PTFE plate ($F_m = G$) with an air gap. Then, the TENG works in a freestanding style. In this situation, the suspended MD can be much more easily driven by the excitations along any directions. As the air gap disappears, even the excitations from the vertical direction also can break the balance, which forces the MD either toward or away from the PTFE plate. That is to say, through analyzing the output signals of the TENG, the vertical motion direction also can be detected.

When the MFMS is horizontally attached with some rotational parts, it cannot realize rotational speed detection. When it is placed on the rotational center, the MD will always stay in the center. When it is eccentrically placed, under the role of centrifugal force, the MD will always stay in the outer region of the PTFE plate. In actual applications, except for the horizontal placement, the MFMS can realize rotational speed detection through introduction of the role of gravity. Compared with commercial angle sensors, is is not necessary to assemble the MFMS with a shaft, which decreases the need for installation and is much more convenient. In the following, the MFMS has been driven by hand to verify the ability of rotational speed detection. When the MD rotates on the PTFE plate, taking clockwise rotation as an example, the simulation results of electrostatic potential and the open-circuit voltage waveforms are shown in Figure 4a,b, respectively. In a period, North-E, East-E, South-E, and West-E reach their maximum output performance in turn, and when the MD rotates anticlockwise, the four arc electrodes reach their maximum output performance in the reverse order, as shown in Figure S5a. From those figures it can be obtained that the arc electrodes output a period waveform with the MD rotates a circle. Thus, the rotational speed can be tested through analyzing the frequency of the arc electrodes' output waveforms. The linear relationship between the rotational speed and the frequency has been plotted in Figure S5b. Based on the time sequence and the frequency of the arc electrodes, a rotation application has been built up to measure the rotational parameters. The whole testing process of the clockwise and anticlockwise rotations has been recorded in Video S1.

In the following, the role of the MFMS for detecting linear acceleration has been analyzed and experimentally tested. When the MD has linear motion along any direction and passes through the inner and outer circle electrodes in turn, the simulation results of the electrostatic potential of two circle electrodes reach each peak in the corresponding turn, as shown in Figure 4c. According to the voltage waveforms of the inner and outer circle electrodes, the relationship between the features of the voltage waveforms and the motion position is shown in Figure 4d. When the MD is at the center, the open-circuit voltages of the two electrodes equal 0 V. When the MD is moving above the inner circle electrode, its open-circuit voltage will reach a trough value. Then, with the MD moving away from the inner circle electrode and toward the outer circle electrode, the open-circuit voltage of the inner circle electrode will increase significantly and manifest a peak value. According to the peak and trough values of the inner circle electrode's voltage waveform, a time parameter recorded as T related to the acceleration can be determined. Since the distance between two circle electrodes is fixed, using an experimental system shown in Figure S6, an exponent relation between T and acceleration has been demonstrated and plotted in Figure 4e. At the same time, the open-circuit voltage of the outer circle electrode reaches a trough value, the amplitude of which has been used to confirm the motion distance of the MD. In order to obtain the accurate linear acceleration, the MD must pass through the inner and outer circle electrodes successively, and the distance between the two circle electrodes determines the minimum value of the linear acceleration (MVLA). Through decreasing the distance, a much smaller MVLA can be obtained by the MFMS. In addition, the MVLA also can be reduced by decreasing the magnetic attractive force. Using magnets with much smaller dimensions to construct the magnetic regulation system is a good choice. At the same time, the distance between the MD and MC also can be increased. According to the software algorithm flowchart described in Figure S7, a LabVIEW-based linear motion application of MFMS has been designed and tested, as shown in Figure 4f and Video S2. In this process, a hand has been used to provide the excitation to the MFMS. Along the same direction, the acceleration under the different state of hand motion has been measured by the MFMS, and the distinguishing ability of eight linear directions has been successively tested and verified in this video.

In the future, except for using magnets with small sizes, the 3D printing and MEMS fabrication technique can also be introduced to manufacture a miniaturized MFMS. After the minimization design and embedding the MFMS in the balance car, the output results of the MFMS can used to control the balance car. Taking the North-E toward the forward direction of the balance car as an example, the result of the north direction can be used to increase the speed, the result of the south direction can be used to decrease the speed, break, and back off, and the results of other directions can be used to turn. Furthermore, the detected acceleration can also be used to control the speed of those processes.

CONCLUSIONS

In summary, a self-powered multifunctional motion sensor enabled by the magnetic-regulated TENG has been designed and fabricated to measure the direction and acceleration of rotation and linear motion simultaneously. The magnetic regulation system through applying a magnetic attraction to the moving part of the MFMS helps it be prepared for the measurement at any time. The sensing capability of multifunctional motion parameters has been analyzed and tested, which also has been verified in two LabVIEW-based motion applications of the MFMS. Based on the two circle electrodes, the MFMS can work as a self-powered 2D acceleration sensor. Under the role of the arc electrodes, the MFMS also can be used as a self-powered rotational parameter sensor and direction sensor. When the MFMS is triggered by linear motion along different directions, the arc electrodes have different voltage outputs, which relates with the corresponding area between the moving part and arc electrodes. This shows that the direction can be measured by the ratio of open-circuit voltages between the arc electrodes. But the corresponding area would not always change significantly, especially when the motion direction is near the center axis of the arc electrode. Thus, in order to ensure the accuracy and reliability of the measurement, the MFMS has been used only to detect eight

DOI: 10.1021/acsnano.8b01589
ACS Nano XXXX, XXX, XXX−XXX

linear motion directions, which can be improved by optimizing the shape of the arc electrodes.

EXPERIMENTAL SECTION

Fabrication of the Friction Layer. The friction layer consisted of a PTFE plate and six electrodes. A PTFE thin film with 3M very high bond adhesive (McMaster-Carr, thickness: 0.002 and 0.0015 in., respectively) was cleaned and cut into a circle with a diameter of 32 mm to make the PTFE plate. A highly conductive copper electrical tape with nonconductive adhesive (McMaster-Carr, thickness: 0.0014 and 0.0015 in., respectively) was cleaned and cut into different dimensions shown in Figure S2a to make the electrodes. To ensure the electrodes can be accurately fixed on the right places of the PTFE plate, an acrylic mask with a thickness of 0.063 in. was made by a laser cutter (PLS6.75, Universal Laser Systems). After connecting the output wires, six acrylic space-filling blocks with the same shapes of electrodes made by the laser cutter were adhered behind the electrodes.

Fabrication of the Shell. The acrylic lid was made by the laser cutter with a 0.063 in. acrylic plate. The acrylic pedestal was adhered by three parts, which were made by the laser cutter with acrylic plates of three different thicknesses of 0.125, 0.25, and 0.35 in.

ASSOCIATED CONTENT

Supporting Information

The Supporting Information is available free of charge on the ACS Publications website at DOI: 10.1021/acsnano.8b01589.

Schematic of the motion sensor; size diagram of the friction layer; simulated results of the magnetic field; mechanics analysis diagram of the magnetic regulation system; voltage waveforms of arc electrodes; relationship between rotational speed and frequency of the arc electrodes' output waveforms; results of the clockwise and anticlockwise rotation; experimental system for testing the relationship between T and acceleration; software algorithm flowchart (PDF)

Rotational parameters detection using MFMS (AVI)

Linear motion parameters detection using MFMS (AVI)

AUTHOR INFORMATION

Corresponding Author

*E-mail: zhong.wang@mse.gatech.edu.

ORCID

Zhong Lin Wang: 0000-0002-5530-0380

Author Contributions

⊥Z. Wu, W. Ding, and Y. Dai contributed equally to this work.

Notes

The authors declare no competing financial interest.

ACKNOWLEDGMENTS

Research was supported by the Hightower Chair Foundation of the Georgia Institute of Technology, the National Natural Science Foundation of China (61503051), the Scientific and Technological Research Program of Chongqing Municipal Education Commission (KJ1600904), and the Natural Science Foundation of Chongqing (cstc2017jcyjAX0124). Z.W. and Y.D. thank the China Scholarship Council for supporting research at Georgia Institute of Technology.

REFERENCES

(1) Hagiwara, N.; Suzuki, Y.; Murase, H. A Method of Improving the Resolution and Accuracy of Rotary Encoders Using a Code Compensation Technique. *IEEE Trans. Instrum. Meas.* **1992**, *41*, 98−101.

(2) Miyashita, K.; Takahashi, T.; Yamanaka, M. Features of a Magnetic Rotary Encoder. *IEEE Trans. Magn.* **1987**, *23*, 2182−2184.

(3) Fleming, A. J. A Review of Nanometer Resolution Position Sensors: Operation and Performance. *Sens. Actuators, A* **2013**, *190*, 106−126.

(4) Heartz, R. A.; Saunders, R. M. Design of High-Precision Synchros and Resolvers. *Trans. Am. Inst. Electr. Eng., Part 2* **1956**, *74*, 421−426.

(5) Bergas-Jané, J.; Ferrater-Simón, C.; Gross, G.; Ramírez-Pisco, R.; Galceran-Arellano, S.; Rull-Duran, J. High-Accuracy All-Digital Resolver-to-Digital Conversion. *IEEE Trans. on Ind. Electron.* **2012**, *59*, 326−333.

(6) Figueiredo, J. Resolver Models for Manufacturing. *IEEE Trans. on Ind. Electron.* **2011**, *58*, 3693−3700.

(7) Shuangfeng, L.; Tiehua, M.; Wen, H. Design and Fabrication of a New Miniaturized Capacitive Accelerometer. *Sens. Actuators, A* **2008**, *147*, 70−74.

(8) Hindrichsen, C. C.; Almind, N. S.; Brodersen, S. H.; Lou-Møller, R.; Hansen, K.; Thomsen, E. V. Triaxial MEMS Accelerometer with Screen Printed PZT Thick Film. *J. Electroceram.* **2010**, *25*, 108−115.

(9) Nemirovsky, Y.; Nemirovsky, A.; Muralt, P.; Setter, N. Design of Novel Thin-Film Piezoelectric Accelerometer. *Sens. Actuators, A* **1996**, *56*, 239−249.

(10) Scarborough, J. B. *The Gyroscope: Theory and Application*; Interscience Pub., 1958.

(11) Lefevre, H. C. *The Fiber-Optic Gyroscope*; Artech House, 2014.

(12) Singh, H. *Compass Routing on Geometric Graphs*; University of Ottawa: Canada, 1999.

(13) Nussinov, Z.; Van Den Brink, J. Compass Models: Theory and Physical Motivations. *Rev. Mod. Phys.* **2015**, *87*, 1.

(14) Akyildiz, I. F.; Su, W.; Sankarasubramaniam, Y.; Cayirci, E. A Survey on Sensor Networks. *IEEE Commun. Mag.* **2002**, *40*, 102−114.

(15) Son, D.; Lee, J.; Qiao, S.; Ghaffari, R.; Kim, J.; Lee, J. E.; Song, C.; Kim, S. J.; Lee, D. J.; Jun, S. W. Multifunctional Wearable Devices for Diagnosis and Therapy of Movement Disorders. *Nat. Nanotechnol.* **2014**, *9*, 397−404.

(16) Hua, Q.; Sun, J.; Liu, H.; Bao, R.; Yu, R.; Zhai, J.; Pan, C.; Wang, Z. L. Skin-Inspired Highly Stretchable and Conformable Matrix Networks for Multifunctional Sensing. *Nat. Commun.* **2018**, *9*, 244.

(17) Ma, M.; Liao, Q.; Zhang, G.; Zhang, Z.; Liang, Q.; Zhang, Y. Self-Recovering Triboelectric Nanogenerator as Active Multifunctional Sensors. *Adv. Funct. Mater.* **2015**, *25*, 6489−6494.

(18) Liao, X.; Liao, Q.; Zhang, Z.; Yan, X.; Liang, Q.; Wang, Q.; Li, M.; Zhang, Y. A Highly Stretchable ZnO@ Fiber-Based Multifunctional Nanosensor for Strain/Temperature/UV Detection. *Adv. Funct. Mater.* **2016**, *26*, 3074−3081.

(19) Lee, J. S.; Shin, K.-Y.; Cheong, O. J.; Kim, J. H.; Jang, J. Highly Sensitive and Multifunctional Tactile Sensor using Free-Standing ZnO/PVDF Thin Film with Graphene Electrodes for Pressure and Temperature Monitoring. *Sci. Rep.* **2015**, *5*, 7887.

(20) Zhang, L.; Jin, L.; Zhang, B.; Deng, W.; Pan, H.; Tang, J.; Zhu, M.; Yang, W. Multifunctional Triboelectric Nanogenerator Based on Porous Micro-Nickel Foam to Harvest Mechanical Energy. *Nano Energy* **2015**, *16*, 516−523.

(21) Wu, Z.; Wen, Y.; Li, P. A Power Supply of Self-Powered Online Monitoring Systems for Power Cords. *IEEE Trans. Energy Convers.* **2013**, *28*, 921−928.

(22) Fan, F.-R.; Tian, Z.-Q.; Lin Wang, Z. Flexible Triboelectric Generator. *Nano Energy* **2012**, *1*, 328−334.

(23) Wang, Z. L. Triboelectric Nanogenerators as New Energy Technology for Self-Powered Systems and as Active Mechanical and Chemical Sensors. *ACS Nano* **2013**, *7*, 9533−9557.

(24) Wang, Z. L. Triboelectric Nanogenerators as New Energy Technology and Self-Powered Sensors−Principles, Problems and Perspectives. *Faraday Discuss.* **2015**, *176*, 447−458.

(25) Wang, Z. L. Catch Wave Power in Floating Nets. *Nature* **2017**, *542*, 159.

DOI: 10.1021/acsnano.8b01589
ACS Nano XXXX, XXX, XXX−XXX

(26) Zhang, L.; Zhang, B.; Chen, J.; Jin, L.; Deng, W.; Tang, J.; Zhang, H.; Pan, H.; Zhu, M.; Yang, W. Lawn Structured Triboelectric Nanogenerators for Scavenging Sweeping Wind Energy on Rooftops. *Adv. Mater.* **2016**, *28*, 1650−1656.
(27) Zhang, H.; Yang, Y.; Su, Y.; Chen, J.; Adams, K.; Lee, S.; Hu, C.; Wang, Z. L. Triboelectric Nanogenerator for Harvesting Vibration Energy in Full Space and as Self-Powered Acceleration Sensor. *Adv. Funct. Mater.* **2014**, *24*, 1401−1407.
(28) Jing, Q.; Zhu, G.; Wu, W.; Bai, P.; Xie, Y.; Han, R. P. S.; Wang, Z. L. Self-Powered Triboelectric Velocity Sensor for Dual-Mode Sensing of Rectified Linear and Rotary Motions. *Nano Energy* **2014**, *10*, 305−312.
(29) Zhang, B.; Zhang, L.; Deng, W.; Jin, L.; Chun, F.; Pan, H.; Gu, B.; Zhang, H.; Lv, Z.; Yang, W. Self-Powered Acceleration Sensor Based on Liquid Metal Triboelectric Nanogenerator for Vibration Monitoring. *ACS Nano* **2017**, *11*, 7440−7446.
(30) Xu, M.; Wang, Y.-C.; Zhang, S. L.; Ding, W.; Cheng, J.; He, X.; Zhang, P.; Wang, Z.; Pan, X.; Wang, Z. L. An Aeroelastic Flutter Based Triboelectric Nanogenerator as a Self-Powered Active Wind Speed Sensor in Harsh Environment. *Extreme Mech. Lett.* **2017**, *15*, 122−129.
(31) Yu, H.; He, X.; Ding, W.; Hu, Y.; Yang, D.; Lu, S.; Wu, C.; Zou, H.; Liu, R.; Lu, C. A Self-Powered Dynamic Displacement Monitoring System Based on Triboelectric Accelerometer. *Adv. Energy Mater.* **2017**, *7*, 1700565.
(32) Wang, P.; Liu, R.; Ding, W.; Zhang, P.; Pan, L.; Dai, G.; Zou, H.; Dong, K.; Xu, C.; Wang, Z. L. Complementary Electromagnetic-Triboelectric Active Sensor for Detecting Multiple Mechanical Triggering. *Adv. Funct. Mater.* **2018**, *28*, 1705808.
(33) Pang, Y. K.; Li, X. H.; Chen, M. X.; Han, C. B.; Zhang, C.; Wang, Z. L. Triboelectric Nanogenerators as a Self-Powered 3D Acceleration Sensor. *ACS Appl. Mater. Interfaces* **2015**, *7*, 19076−19082.
(34) Wen, Z.; Guo, H.; Zi, Y.; Yeh, M.-H.; Wang, X.; Deng, J.; Wang, J.; Li, S.; Hu, C.; Zhu, L.; Wang, Z. L. Harvesting Broad Frequency Band Blue Energy by a Triboelectric−Electromagnetic Hybrid Nanogenerator. *ACS Nano* **2016**, *10*, 6526−6534.
(35) Wang, X.; Wen, Z.; Guo, H.; Wu, C.; He, X.; Lin, L.; Cao, X.; Wang, Z. L. Fully Packaged Blue Energy Harvester by Hybridizing a Rolling Triboelectric Nanogenerator and an Electromagnetic Generator. *ACS Nano* **2016**, *10*, 11369−11376.
(36) Shao, H.; Wen, Z.; Cheng, P.; Sun, N.; Shen, Q.; Zhou, C.; Peng, M.; Yang, Y.; Xie, X.; Sun, X. Multifunctional Power Unit by Hybridizing Contact-Separate Triboelectric Nanogenerator, Electromagnetic Generator and Solar Cell for Harvesting Blue Energy. *Nano Energy* **2017**, *39*, 608−615.

DOI: 10.1021/acsnano.8b01589
ACS Nano XXXX, XXX, XXX−XXX